Chin-Yin Hsu[a], Teng-Chun Yang[a], Tung-Lin Wu, Ke-Chang Hung and Jyh-Horng Wu*

Effects of a layered structure on the physicomechanical properties and extended creep behavior of bamboo-polypropylene composites (BPCs) determined by the stepped isostress method

https://doi.org/10.1515/hf-2017-0165
Received October 16, 2017; accepted March 5, 2018; previously published online April 6, 2018

Abstract: A layered bamboo-plastic composite (BPC) consisting of bamboo (*Phyllostachys makinoi*) particles and polypropylene was investigated. The influence of the layering conditions, including the thickness and bamboo content in various layers, was the focus in terms of the physicomechanical and creep properties of the BPCs. The results showed that a three-layered BPC (BPC_{3L}) with a 1:3:1 thickness ratio and with top/bottom layer containing 40% bamboo exhibited the best specific flexural properties. An accelerated creep test approach was applied, known as the short-term stepped isostress method (SSM), to predict the long-term creep behavior of BPC_{3L}. The results indicated that the creep master curves, which are constructed from different SSM testing parameters, agree well with the long-term experimental creep data and that the creep resistance of homogeneous single-layered BPC was better than that of BPC_{3L}.

Keywords: bamboo particle, creep behavior, layered structural composite, polypropylene, stepped isostress method

Introduction

Natural fibers in composites – such as the fibers of wood, bamboo, flax, ramie, jute, kenaf and hemp – have numerous advantages, including low density, high toughness, good specific strength properties, renewability and biodegradability (Xu et al. 2001; Zhang et al. 2002; Oksman et al. 2003; Klyosov 2007; Lee et al. 2010; Kumar et al. 2011; Dittenber and Ganga Rao 2012; Saba et al. 2015). Bamboo fibers (BFs) have excellent properties (Wang et al. 2014, 2016; Li et al. 2015, 2017; Liu et al. 2015a,b) and may also improve the properties of polymer composites due to their excellent characteristics (Yang et al. 2009; Yu et al. 2011; Cheng et al. 2015; Liu et al. 2015a,b). The availability of BFs across Asia is good with an increasing tendency (Scurlock et al. 2000). However, a major drawback of BFs is their hygroscopicity and incompatibility with the hydrophobic thermoplastics in bamboo-plastic composites (BPCs). To improve this situation, research activities focused on the modification of fibers by physical and chemical methods, such as heat treatment, esterification, alkaline treatment, steam explosion treatment and the application of coupling agents (Rowell 1983; Deshpande et al. 2000; Keener et al. 2004; Okubo et al. 2004; Das and Chakraborty 2008; Hung and Wu 2010; Cheng et al. 2015).

In engineering materials and polymer composites, multi-layered structures proved of high value as each separate layer can be optimized and thus an efficient load bearing can be achieved, which is better than that of a conventional homogeneous single-layered structure (Altenbach 1998). Layered particleboards and fiberboards in the field of wood based composites are examples of composites, which have higher bending strength and stiffness compared to the homogenous counterparts at the same level of density. Kazemi et al. (2013) determined the effects of a three layered wood-plastic composite (WPC_{3L}) in terms of their mechanical properties as a function of wood particle content, layer thickness, stacking sequence in symmetric and asymmetric configurations.

BPC is susceptible to time-dependent deformation when subjected to loading and this load-bearing capacity must be known for engineering applications. On the other hand, long-term creep tests are expensive, and therefore master curves obtained from a short-term accelerated creep test in combination with an empirical mathematical model are less expensive and useful in this context. This approach is based on the superposition principle consisting of parameters exposure time and temperature and different loads. According to the time-temperature superposition principle (TTSP), the creep behavior of viscoelastic materials can be determined from the stepped temperature in the same way as

[a]**Chin-Yin Hsu and Teng-Chun Yang:** These authors contributed equally to this work.
***Corresponding author: Jyh-Horng Wu,** Department of Forestry, National Chung Hsing University, Taichung 402, Taiwan, e-mail: eric@nchu.edu.tw
Chin-Yin Hsu, Teng-Chun Yang, Tung-Lin Wu and Ke-Chang Hung: Department of Forestry, National Chung Hsing University, Taichung 402, Taiwan

time-equivalence (Dasappa et al. 2009; Hung et al. 2015; Yang et al. 2015). Furthermore, the stepped isothermal method (SIM), which was developed from TTSP, is based on stepped increments of temperature for a single sample (Jones and Clarke 2007; Alwis and Burgoyne 2008; Yeo and Hsuan 2010; Achereiner et al. 2013). The stepped isostress method (SSM), which is a derivative method of SIM, captures the creep behavior acceleration of a single sample with the stepwise increase of the stress level (Hadid et al. 2004; Giannopoulos and Burgoyne 2011, 2012; Hadid et al. 2014; Tanks et al. 2017). The SSM approach has several advantages for polymer composites compared to SIM (Hadid et al. 2014) because the temperature is constant and thus the material properties are not affected by this parameter and the non-uniform heating of thick polymeric materials with low thermal conductivity, is prevented. The long-term creep behavior of aramid yarns was predicted successfully (Giannopoulos and Burgoyne 2011, 2012) by this approach, which is also true for semi-crystalline thermoplastics (Hadid et al. 2004, 2014), and carbon fiber reinforced polymer (Tanks et al. 2017). Little information is available on the SSM method for characterizing creep deformation and predicting the long-term creep behavior of BPCs. The goal of the present paper is to fill this gap. The effects of layering design will be investigated on the physicomechanical properties of three-layered structural BPCs, while the time-stress dependent response (the extended creep behavior) of this material will be checked based on the SSM approach.

Materials and methods

Materials: Bamboo particles (BPs) were prepared from a 3-year-old Makino bamboo (*Phyllostachys makinoi* Hayata), which was provided by the local bamboo-processing factory, and which are obtained via hammer-milling and sieving. The particle size is between 6 and 16 mesh (3.35–1.18 mm). Commercially available polypropylene (PP) pellets (Yung Chia Chemical Industries Co., Ltd., Taipei, Taiwan) were ground in an attrition mill to reduce their particle size to 20–80 mesh (180–850 μm). Properties of PP: 915 kg m^{-3}, 145°C m.p. and 4–8 g per 10 min melt flow index.

Composite panel manufacture: Homogeneous (single-layered) BPC_H and three-layered BPC_{3L} were manufactured (see Figure 1). In BPC_{3L}, the thickness ratios are 1:2:1, 1:3:1 and 1:4:1. Additionally, the BP contents in the top/bottom layer were 20, 30 and 40%. The ratio of oven-dried BP to PP powder was fixed at 1/1 by wt. in the whole BPCs and the BP/PP ratio in the core layer was distributed. The sample coding system of WPC_{3L} was described as LXXX-YY, where XXX and YY represent the thickness ratio and BP content (%) in both the top and bottom layers, respectively, as presented in Table 1. The expected density of all BPCs was 800 kg m^{-3} and the BPC samples had thickness values of 12 mm. All BPCs were compression molded in a two-step pressing process as follows: (1) hot pressing at 200°C under a load of 2.5 MPa; (2) finishing based on cold pressing until the temperature of the BPCs decreased to 40°C.

Characterization methods: Physicomechanical properties were determined according to the Chinese National Standard CNS 2215, including density, water absorption (WAbs), thickness swelling (ThSw), modulus of rupture (MOR), modulus of elasticity (MOE) and wood screw holding strength (ScrHS). Flexural properties (MOR and MOE) were obtained from samples with dimensions of

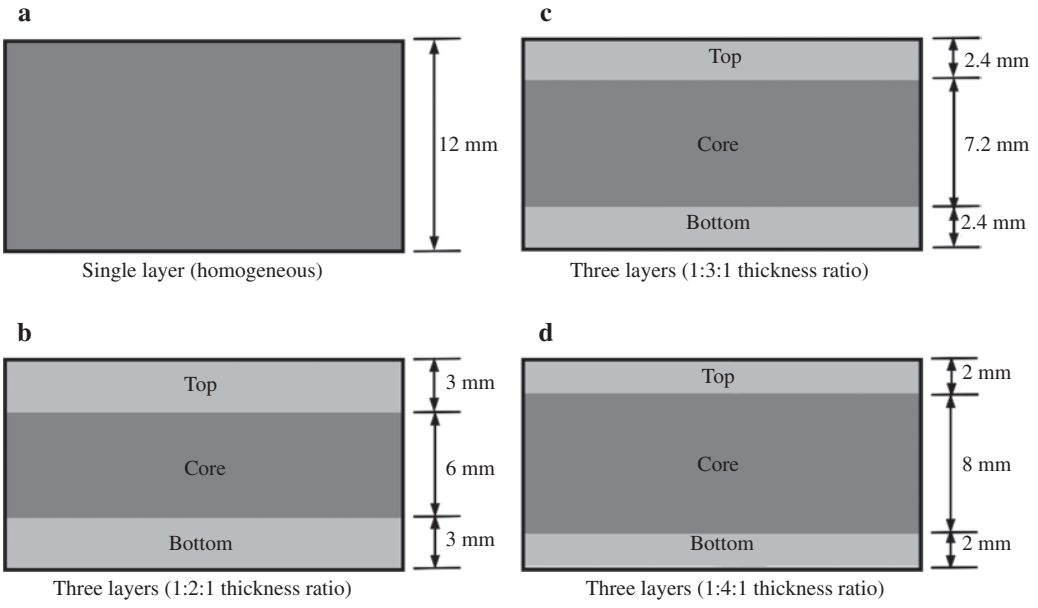

Figure 1: Schematic diagrams of various BPCs.
Homogeneous single-layered (a) and three-layered BPCs with a 1:2:1 thickness ratio (L121) (b), 1:3:1 thickness ratio (L131) (c), and 1:4:1 thickness ratio (L141) (d).

230 mm × 50 mm × 12 mm using the three-point static bending test with a loading speed of 10 mm min^{-1} and a span of 180 mm. The ScrHS was determined (sample size: 50 mm × 50 mm × 12 mm) with a tensile speed of 2 mm min^{-1}. For density profile analysis, each layer of BPCs with dimensions of 50 mm × 50 mm × 12 mm was cut off gradually with a circular sawing machine, and the weight loss (WL) and volume residue (VR) were measured. Accordingly, the vertical density profile was calculated based on the WL per volume. All samples were conditioned at 20°C and 65% relative humidity (RH) for 2 weeks prior to testing, and five samples of each BPC were tested.

Short-term accelerated creep tests: The short-term SSM was implemented in a universal testing machine (Shimadzu AG-10kNX, Tokyo, Japan). The creep strain is defined as:

$$\varepsilon(\sigma_r, t) = \varepsilon(\sigma, t/\alpha_\sigma) \quad (1)$$

where ε is the creep strain as a function of stress and time, σ_r is the reference stress, σ is the elevated stress and α_σ is the shift factor. The reference stress: 20% of the average breaking load (ABL); dwell time: 2 h for each isostress. Creep tests were conducted in the isostress range between 20 and 75% ABL at intervals of 5% ABL. Additionally, different SSM testing parameters were implemented to see the differences between the SSM creep tests. The stepwise stress increments: 5, 7.5, 10 and 12.5% ABL; the dwell times: 2, 3 and 5 h.

The activation volume was calculated based on the Eyring model in Eq. (2), which is well suited for the description of the creep behavior of a polymer composite below the glass transition temperature. This equation and was applied, for example, to estimate the shift factor (α_σ), which shows the express rate with the stress level (Giannopoulos and Burgoyne 2011; Hadid et al. 2014):

$$\log \alpha_\sigma = \log\left(\frac{\dot{\varepsilon}}{\dot{\varepsilon}_r}\right) = \frac{V^*}{2.303kT}(\sigma - \sigma_r) \quad (2)$$

where $\dot{\varepsilon}$ is the creep rate at the elevated stress (σ), $\dot{\varepsilon}_r$ is the creep rate at the reference stress (σ_r), V^* is the activation volume, k is Boltzmann's constant and T is the absolute temperature.

Full-scale experimental creep tests: For validation of the SSM master curves the applied stress was 20% ABL, and the mid-span deflection values of the samples were measured and recorded by means of a linear variable differential transducer (LDVT) for a 90-day period. All samples were held at 20°C and 65% RH, and three samples of each BPC were tested.

Analysis of variance: All of the results are expressed in terms of the mean ± SD. The significance of differences was calculated by Student's t-test.

Results and discussion

Physical properties

The density for all of the composites ranged from 806 to 841 kg m^{-3} (Table 1), indicating that the actual density is higher than the expected one (800 kg m^{-3}). This result is attributable to the reduction of the composite size after BPC_{3L} manufacturing due to the higher shrinkage of semi-crystalline PP during the cooling step. It can also be observed that the BPC_{3L} with 20% BP in the top/bottom layers (i.e. L121-20, L131-20 and L141-20) had the lowest density among the various layer configurations. It can be speculated that BPC_{3L}s with high BP content in the core layer leads to less matrix shrinkage of the composites.

WAbs and ThSw were measured after 24 h of soaking (Table 1). As an example of a 1:2:1 thickness ratio for BPC_{3L}s, WAbs increased from 4.0 (BPC_H) to 10.5% and to 19.0% for L121-30 and L121-20, respectively. One factor influencing WAbs is the size of lumens and fine pores, as they have

Table 1: Composition, construction and physicomechanical properties of various BPCs.

		Top/bottom layer		Core layer			24 h Soaking		Flexural properties		
Code	Thickness ratio	BP (%)	PP (%)	BP (%)	PP (%)	Density (kg m^{-3})	WAbs (%)	ThSw (%)	sMOR (MPa)	sMOE (GPa)	sScrHS (kN)
BPC_H	–	50	50	50	50	834 ± 4	4.0 ± 0.4	1.7 ± 0.1	30.3 ± 1.0	2.74 ± 0.13	1.44 ± 0.05
L121-20	1:2:1	20	80	80	20	819 ± 9^a	19.0 ± 1.0^b	6.2 ± 1.1^b	32.1 ± 1.1	2.60 ± 0.1	1.09 ± 0.05^b
L121-30		30	70	70	30	837 ± 7	10.5 ± 1.7^b	2.8 ± 0.4^a	32.8 ± 1.0	2.73 ± 0.07	1.30 ± 0.03^b
L121-40		40	60	60	40	841 ± 9	3.8 ± 0.8	1.7 ± 0.2	32.4 ± 0.9^a	2.86 ± 0.05	1.53 ± 0.07^a
L131-20	1:3:1	20	80	70	30	817 ± 7^b	12.6 ± 1.6^b	3.1 ± 0.3^b	32.8 ± 0.8^b	2.81 ± 0.08	1.28 ± 0.07^b
L131-30		30	70	64	36	824 ± 9^a	6.3 ± 2.3^a	2.0 ± 0.2	33.0 ± 0.6^b	2.79 ± 0.09	1.33 ± 0.06
L131-40		40	60	57	43	826 ± 4^a	3.8 ± 0.4	1.6 ± 0.2	33.4 ± 1.3^b	2.89 ± 0.07^a	1.37 ± 0.04
L141-20	1:4:1	20	80	65	35	806 ± 17^a	6.9 ± 1.6^b	1.7 ± 0.2	28.9 ± 0.7^a	2.59 ± 0.17	1.42 ± 0.05
L141-30		30	70	60	40	831 ± 16	5.7 ± 2.6^b	2.0 ± 0.6	31.2 ± 2.0	2.64 ± 0.06	1.49 ± 0.03
L141-40		40	60	55	45	824 ± 8^a	4.0 ± 0.5	1.5 ± 0.3	29.6 ± 1.1	2.60 ± 0.11	1.55 ± 0.09^a

Weight ratio of BP/PP in all BPCs is 1/1.

Values are the mean ± SD (n = 5). $^aP < 0.05$; $^bP < 0.001$; compared with BPC_H.

WAbs, Water absorption; ThSw, thickness swelling; sMOR, specific modulus of rupture; sMOE, specific modulus of elasticity; sScrHS, specific wood screw holding strength.

an effect on the access of water to the hydrophilic OH groups of the cell wall, especially to those of hemicelluloses within the cell wall (Ashori and Sheshmani 2010). The second factor is attributed to the gaps and flaws at the BP-polymer matrix interface and the microcracks in the polymer matrix, which are formed during the process (Espert et al. 2004; Adhikary et al. 2008). Water diffusion blockage may also occur for high density composites produced under high compression and with a high filling moiety during processing (Clemons and Idach 2004). Based on the above mentioned factors, L121-20 exhibited the highest WAbs at the same thickness ratio of BPC_{3L} as it has the lowest density (819 kg m^{-3}) and highest BP content (80%) in the core layer. However, such BPC_{3L}s dispose of WAbs values in the top/bottom layer around 19.0, 12.6 and 6.9% for L121-20, L131-20 and L141-20, respectively. Accordingly, thickness decrement in the core layer and an increment of the BP content in the core layers led to an increase of WAbs. However, except for L141, the ThSw shows the same tendency as WAbs. For instance, L121-20 exhibited the highest ThSw (6.2%) among all of the BPCs and it has the highest BP content in the core layer. For the vertical density profiles of various BPCs, as shown in Figure 2, it is expected that the density of BPC_H would be consistent, while the density of BPC_{3L}s in the top/bottom layers would be higher than that in the core layer.

Mechanical properties

The BPC_H and BPC_{3L} composites have significant differences in their vertical density profiles, and this should have consequences for their mechanical properties. Table 1 presents the flexural properties and ScrHS of various BPCs. The specific strength formed the basis for estimating the mechanical properties. It can be seen that the specific MOR (sMOR) data for all composites ranged from 28.9 to 33.4 MPa. Among them, L131-40 had the highest sMOR (33.4 MPa), while L141-40 had the lowest one (28.9 MPa). Compared with BPC_H, the sMOR of L121-40 and L131-40 significantly increased by 7.0 and 9.1%, respectively. Obviously, layered structures can improve the flexural strength of a composite. A similar result was reported by Abdel-Mohti et al. (2015). Additionally, L121 had a lower sMOR than that of L131. According to Verhey et al. (2001), Chen et al. (2006) and Hung and Wu (2010), the flexural properties of BPC_Hs do not increase with an increasing fiber content, probably because of the poor dispersion of fibers, which causes inefficient stress transfer (Adhikary et al. 2008) and a diminished wettability of the polymer matrix (Luo and Netravail 1999). Because the BP content

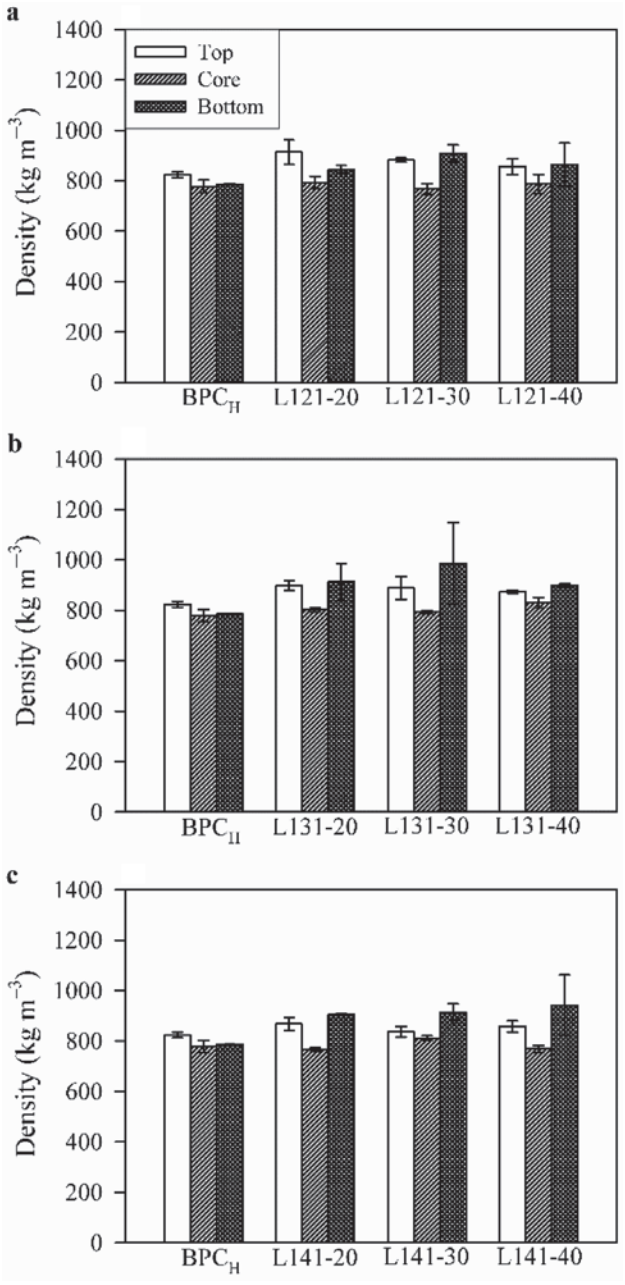

Figure 2: Density profiles of various BPCs.
Homogeneous single-layered and three-layered BPCs with a 1:2:1 thickness ratio (a), 1:3:1 thickness ratio (b), and 1:4:1 thickness ratio (c).

in the core layer of L141 is similar to that of BPC_H, their sMOR values do not differ significantly. However, the sMOEs of all composites ranged from 2.59 to 2.89 GPa. L131-40 had the highest sMOE (2.89 GPa), which was significantly different to that of BPC_H. By contrast, the sMOE for all L141 was approx. 2.6 GPa, which was lower than that of BPC_H (2.74 GPa). It can also be seen that sMOE decreased with increasing PP content in the top/bottom layers, especially in the composite L121. Thus the poor

wettability of the core layer of the PP matrix leads to less sMOE data (Luo and Netravail 1999). The sScrHS data in Table 1, demonstrates: the highest sScrHS was observed for L141 over the range of 1.42–1.55 kN among all BPC_{3L}s, and the sScrHS decreased with decreasing BP contents in the top/bottom layer. These results indicate that L131 as BPC_{3L} has the best mechanical properties.

Accelerated creep via SSM

The composite L131-40 with the best flexural properties (sMOR and sMOE) was selected as an example to outline SSM and long-term creep tests (Table 1). As shown in Figure 3a, the SSM creep curve of BPC_H was produced by the loading sequence of the SSM testing procedure with 20% ABL as reference and a 5% stepwise jump stress with 2-h dwell time. The master curve was constructed based on the four parts of the sequence to analyze the SSM raw data: (1) vertical shifting, (2) rescaling, (3) eliminating and (4) horizontal shifting.

An SSM creep curve shows an immediate strain jump between the load steps. This result implies that there is no creep strain at each jump because of the elasticity of the polymer composites under instantaneous strain. These jumps should be subtracted by vertical shifting to eliminate the elastic component in the recorded strain. This shifting links the start of the current curve to the

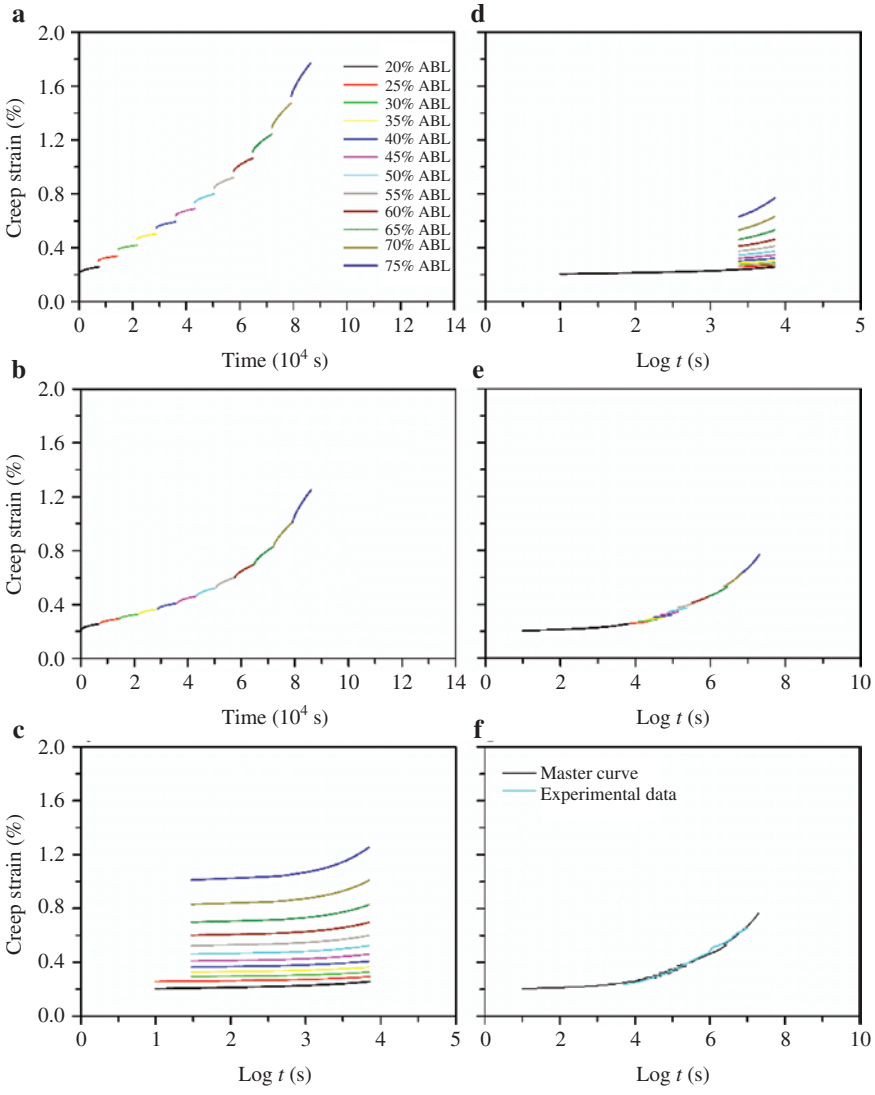

Figure 3: The creep master curve construction for the BPC_H by the SSM.
(a) SSM creep strain of the BPC_H (reference stress: 20% ABL; interval stress: 5% ABL; dwelling time: 2 h). The handling of the test's data of the SSM method for BPC_H: (b) vertical shifting, (c) rescaled creep curves, (d) eliminating before the onset time of each stress step, and (e) horizontal shifting. (f) Experimental data and master curve.

end of the previous curve at each load step, and finally, a continuous creep strain curve is created (Figure 3b). Rescaling was carried out because of the stress and strain history, which included deformation and damage from previous steps. Several rescaling operations were proposed in previous studies (Hadid et al. 2004, 2014; Giannopoulos and Burgoyne 2011, 2012; Tanks et al. 2017). Giannopoulos and Burgoyne (2011) recommended a purely graphic approach. However, the authors suggested that a power law fit (Hadid et al. 2014) or a Prony series fit (Tanks et al. 2017) can be used for curve fitting for the secondary segment of each creep step. In the present study, a rescaling process was implemented, which was described by Yeo and Hsuan (2009). First, as shown in Figure 3c, a series of independent creep curves resulting from a step-wise sequential loading were transited to the reference stress level over a long period of time. Second, Figure 3d shows the elimination of the time before the onset time and creep strain for an individual curve, which is the primary creep region and which is influenced by the stress level and history. After rescaling and eliminating, the individual creep curves should be horizontally transited along the time axis to construct the master curve according to the shift factor, $\log(\alpha_\sigma)$, for a reduced time, the magnitude of which is a function of the stress level. The complete smooth master curve is shown in Figure 3e.

An experimental creep test was performed at 20°C and 65% RH for a period of 90 days for comparison to the short-term SSM test. As seen in Figure 3f, the SSM-predicted creep master curve fits well with the long-term experimental data. The effects of the test conditions (stress increment and dwelling time) on the SSM master curves for BPC_H and BPC_{3L} are presented in Figure 4a and b, respectively. Obviously, both master curves were not influenced by different stress increments and dwelling time variations, and therefore, SSM test results are applicable for the prediction of long-term creep behavior. Figure 4c and d illustrate the relationship between the shift factor and stress level. A linear regression of the slope resulted in the coefficients of determination (R^2) of 0.9744 (BPC_H) and 0.9512 (BPC_{3L}). These results can be safely interpreted that the same creep mechanism is valid for each load sequence, and that the superposition method implemented in the SSM approach is validated for the construction of the creep master curve. The activation

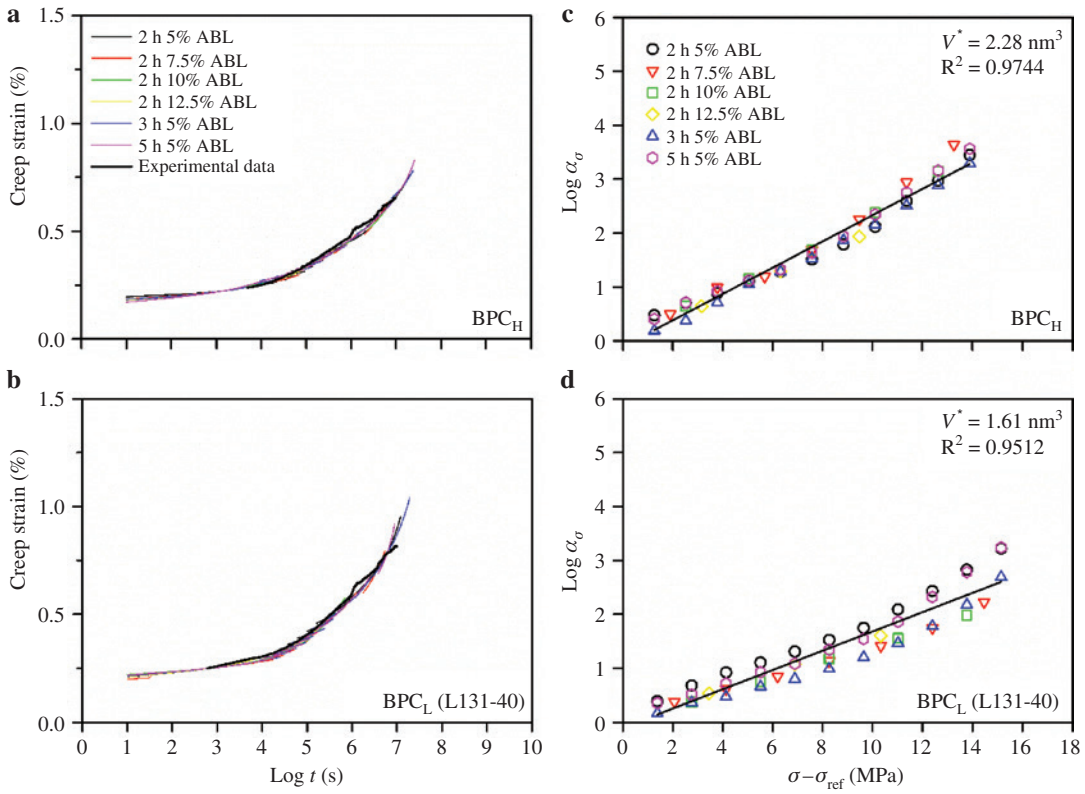

Figure 4: The SSM creep curves of BPCs.
Master curves (a, b) and relationships between the time-stress shift factor and stress level (c, d) of BPC_H and BPC_L from different SSM testing parameters.

volume V^* was calculated from the linear slope of the plot of $\log(\alpha_\sigma)$ vs. $(\sigma - \sigma_r)$ using Eq. (2). Accordingly, V^* of BPC_H (2.28 nm^3) is higher than that of BPC_{3L} (1.61 nm^3). This means that BPC_H requires more stress-work to overcome the activation energy barrier of an incremental deformation of the amorphous segment of the polymer matrix (Raghavan and Meshii 1994, 1998).

Table 2: Parameters of the exponential growth equation for the SSM-predicted creep strain value for BPCs.

Code	ε_0 (%)	a	b	R^2
BPC_H	0.1521	0.0124	0.5311	0.9966
BPC_{3L}	0.1827	0.0124	0.5764	0.9973

$\varepsilon(t) = \varepsilon_0 + ae^{bt}$, where $\varepsilon(t)$ is the time-dependent strain, ε_0 is the instantaneous elastic strain, a and b are constant numbers.

SSM-predicted creep curves

The SSM master curves of BPC_H and BPC_{3L} on a log time scale are presented in Figure 5a. BPC_H has a lower creep strain during the creep time. This is consistent with the results from the activation volume, which were described in the section above, i.e. the creep resistance of the BPC_{3L} is not better, although it has better flexural properties BPCs (Table 1). Additionally, an exponential equation with three parameters was created to fit the creep master curves. As is visible in Figure 5a, the model fits the SSM master curves with R^2 values of 0.9966 (BPC_H) and 0.9973 (BPC_{3L}). The fitted parameters of the exponential equation are listed in Table 2. The SSM-predicted creep curves are illustrated in Figure 5b on a normal time scale. The b value affects the increment rate of creep strain. As shown in Table 2, BPC_{3L} has a b value of 0.5764 compared to that of BPC_H (0.5311). Accordingly, BPC_{3L} has a higher creep rate and a lower creep resistance.

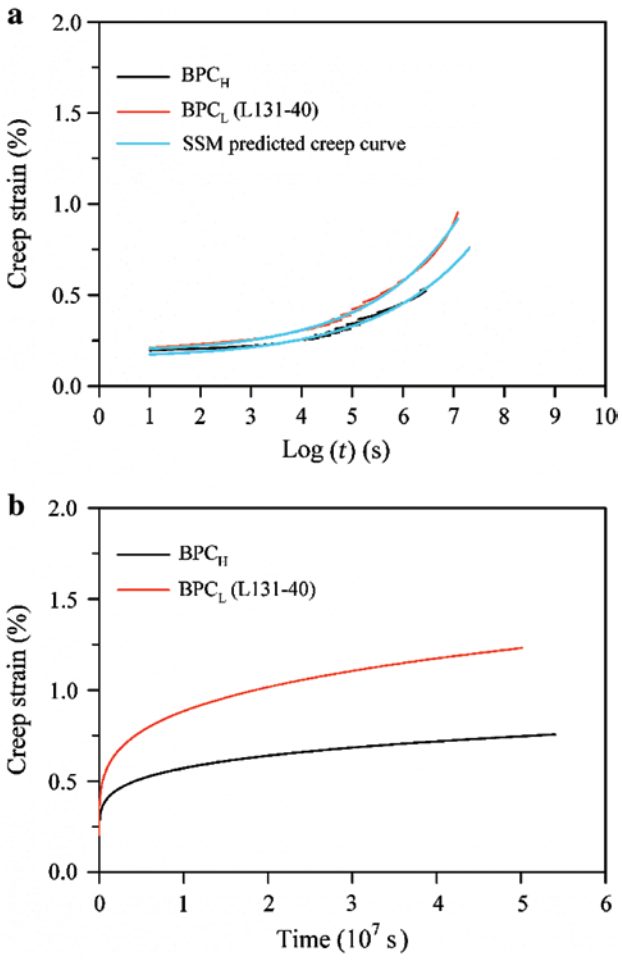

Figure 5: SSM predicated creep curves of BPCs.
The curves on a log time scale (a) and normal time scale (b).

Conclusions

Among all BPC_{3L}s, the composite L141 exhibits the lowest WAbs and highest ThSw. Additionally, WAbs decreased with the increasing BP content in the top/bottom layers. By contrast, the sScrHS increased with the increasing BP content in the top/bottom layer. Among all BPCs, L141-40 had the highest sScrHS (1.55 kN), while L131-20 showed the highest sMOR (33.4 MPa) and sMOE (2.89 GPa). The results reveal that the short-term SSM master curves fit well with the 90-day experimental creep data. In comparison with BPC_{3L}, BPC_H has a lower creep strain during the creep time, indicating that BPC_H has a better creep resistance than the BPC_{3L}. These results provide information regarding the layering conditions and prove that the long-term creep behavior of bamboo fiber PP composites can be predicted by the SSM approach.

Acknowledgments: This work was financially supported by the research grant from the Ministry of Science and Technology, Taiwan (MOST 105-2628-B-005-002-MY3).

Author contributions: All the authors have accepted responsibility for the entire content of this submitted manuscript and approved submission.
Research funding: The Ministry of Science and Technology of Taiwan (MOST 105-2628-B-005-002-MY3).
Employment or leadership: None declared.
Honorarium: None declared.

References

Abdel-Mohti, A., Garbash, A.N., Almagahwi, S., Shen, H. (2015) Effect of layer and film thickness and temperature on the mechanical property of micro- and nano-layered PC/PMMA films subjected to thermal aging. Materials 8:2062–2075.

Achereiner, F., Engelsing, K., Bastian, M., Heidemeyer, P. (2013) Accelerated creep testing of polymers using the stepped isothermal method. Polym. Testing 32:447–454.

Adhikary, K.B., Pang, S., Staiger, M.P. (2008) Dimensional stability and mechanical behavior of wood-plastic composites based on recycled and virgin high-density polyethylene (HDPE). Compos. Part B 39:807–815.

Altenbach, H. (1998) Theories for laminated and sandwich plates. Mech. Compos. Mater. 34:243–252.

Alwis, K.G.N.C., Burgoyne, C.J. (2008) Accelerated creep testing for aramid fibres using the stepped isothermal method. J. Mater. Sci. 43:4789–4800.

Ashori, A., Sheshmani, S. (2010) Hybrid composites made from recycled materials: moisture absorption and thickness swelling behavior. Bioresour. Technol. 101:4717–4720.

Chen, H.C., Chen, T.Y., Hsu, C.H. (2006) Effects of wood particle size and mixing ratios of HDPE on the properties of the composites. Eur. J. Wood Wood Prod. 64:172–177.

Cheng, H., Gao, J., Wang, G., Shi, S.Q., Zhang, S., Cai, L. (2015) Enhancement of mechanical properties of composites made of calcium carbonate modified bamboo fibers and polypropylene. Holzforschung 69:215–221.

Clemons, C.M., Idach, R.E. (2004) Effects of processing method and moisture history on laboratory fungal resistance of wood-HDPE composites. Forest Prod. J. 54:50–57.

Das, M., Chakraborty, D. (2008) Evaluation of improvement of physical and mechanical properties of bamboo fibres due to alkali treatment. J. Appl. Polym. Sci. 107:522–527.

Dasappa, P., Lee-Sullivan, P., Xiao, X. (2009) Temperature effects on creep behavior of continuous fiber GMT composites. Compos. Part A 40:1071–1081.

Deshpande, A.P., Bhaskar Rao, M., Laksjmana Rao, C. (2000) Extraction of bamboo fibers and their use as reinforcement in polymeric composites. J. Appl. Polym. Sci. 76:83–92.

Dittenber, D.B., Ganga Rao, H.V.S. (2012) Critical review of recent publications on use of natural composites in infrastructure. Compos. Part A 43:1419–1429.

Espert, A., Vilaplana, F., Karlsson, S. (2004) Comparison of water absorption in natural cellulosic fibres from wood and one-year crops in polypropylene composites and its influence on their mechanical properties. Compos. Part A 35:1267–1276.

Giannopoulos, I.P., Burgoyne, C.J. (2011) Prediction of the long-term behaviour of high modulus fibres using the stepped isostress method (SSM). J. Mater. Sci. 46:7660–7671.

Giannopoulos, I.P., Burgoyne, C.J. (2012) Accelerated and real-time creep and creep-rupture results for aramid fibers. J. Appl. Polym. Sci. 125:3856–3870.

Hadid, M., Rechak, S., Tati, A. (2004) Long-term bending creep behavior prediction of injection molded composite using stress-time correspondence principle. Mater. Sci. Eng. A 385:54–58.

Hadid, M., Guerira, B., Bahri, M., Zouani, A. (2014) Assessment of the stepped isostress method in the prediction of long term creep of thermoplastics. Polym. Testing 34:113–119.

Hung, K.-C., Wu, J.-H. (2010) Mechanical and interfacial properties of plastic composite panels made from esterified bamboo particles. J. Wood Sci. 56:216–221.

Hung, K.-C., Wu, T.-L., Chen, Y.-L., Wu, J.-H. (2015) Assessing the effect of wood acetylation on mechanical properties and extended creep behavior of wood/recycled-polypropylene composites. Constr. Build. Master. 108:139–145.

Jones, C.J.F.P., Clarke, D. (2007) The residual strength of geosynthetic reinforcement subjected to accelerated creep testing and simulated seismic events. Geotext. Geomembr. 25:155–169.

Kazemi, Y., Cloutier, A., Rodrigue, D. (2013) Design analysis of three-layered structural composites based on post-consumer recycled plastics and wood residues. Compos. Part A 53:1–9.

Keener, T.J., Stuart, R.K., Brown, T.K. (2004) Maleated coupling agents for natural fibre composites. Compos. Part A 35:357–362.

Klyosov, A. Wood-Plastic Composites. John Wiley & Sons, New Jersey, 2007.

Kumar, V., Tyagi, L., Sinha, S. (2011) Wood flour – reinforced plastic composites: a review. Rev. Chem. Eng. 27:253–264.

Lee, C.-H., Wu, T.-L., Chen, Y.-L., Wu, J.-H. (2010) Characteristics and discrimination of five types of wood-plastic composites by Fourier transform infrared spectroscopy combined with principal component analysis. Holzforschung 64:699–704.

Li, Y., Yin, L., Huang, C., Meng, Y., Fu, F., Wang, S., Wu, Q. (2015) Quasi-static and dynamic nanoindentation to determine the influence of thermal treatment on the mechanical properties of bamboo cell walls. Holzforschung 69:909–914.

Li, Y., Huang, C., Wang, L., Wang, S., Wang, X. (2017) The effects of thermal treatment on the nanomechanical behavior of bamboo (*Phyllostachys pubescens* Mazel ex H. de Lehaie) cell walls observed by nanoindentation, XRD, and wet chemistry. Holzforschung 71:129–135.

Liu, H., Jiang, Z., Fei, B., Hse, C., Sun, Z. (2015a) Tensile behaviour and fracture mechanism of moso bamboo (*Phyllostachys pubescens*). Holzforschung 69:47–52.

Liu, W., Chen, T., Xie, T., Lai, F., Qiu, R. (2015b) Oxygen plasma treatment of bamboo fibers (BF) and its effects on the static and dynamic mechanical properties of BF-unsaturated polyester composites. Holzforschung 69:449–455.

Luo, S., Netravail, A.N. (1999) Interfacial and mechanical properties of environment-friendly "green" composites made from pineapple fibers and poly(hydroxybutyrate-co-valerate) resin. J. Mater. Sci. 34:3709–3719.

Oksman, K., Skrifvars, M., Selin, J.F. (2003) Natural fibres as reinforcement in polylactic acid (PLA) composites. Compos. Sci. Technol. 63:1317–1324.

Okubo, K., Fujii, T., Yamamoto, Y. (2004) Development of bamboo-based polymer composites and their mechanical properties. Compos. Part A 35:377–383.

Raghavan, J., Meshii, M. (1994) Activation theory for creep of matrix resin and carbon fiber-reinforced polymer composites. J. Mater. Sci. 29:5078–5084.

Raghavan, J., Meshii, M. (1998) Creep of polymer composites. Compos. Sci. Technol. 57:1673–1688.

Rowell, R.M. (1983) Chemical modification of wood. For. Prod. Abstr. 6:363–382.

Saba, N., Paridah, M.T., Jawaid, M. (2015) Mechanical properties of kenaf fibre reinforced polymer composite: a review. Constr. Build. Mater. 76:87–96.

Scurlock, J.M.O., Dayton, D.C., Hames, B. (2000) Bamboo: an overlooked biomass resource? Biomass Bioenerg. 19:229–244.

Tanks, J.D., Rader, K.E., Sharp, S.R. (2017) Accelerated creep and creep-rupture testing of transverse unidirectional carbon/epoxy lamina based on the stepped isostress method. Compos. Struct. 159:455–462.

Verhey, S.A., Laks, P.E., Richter, D.L. (2001) The effect of composition on the decay resistance of model woodfiber-thermoplastic composites. In: Sixth International Conference on Woodfiber-Plastic Composites, Madison, Wisconsin. pp. 79–86.

Wang, H., An, X., Li, W., Wang, H., Yu, Y. (2014) Variation of mechanical properties of single bamboo fibers (*Dendrocalamus latiflorus* Munro) with respect to age and location in culms. Holzforschung 68:291–297.

Wang, H., Zhang, X., Jiang, Z., Yu, Z., Yu, Y. (2016) Isolating nanocellulose fibrills from bamboo parenchymal cells with high intensity ultrasonication. Holzforschung 70:401–409.

Xu, B., Simonsen, J., Rochefort, W.E. (2001) Creep resistance of wood-filled polystyrene/high-density polyethylene blends. J. Appl. Polym. Sci. 79:418–425.

Yang, G., Zhang, Y., Shao, H., Hu, X. (2009) A comparative study of bamboo Lyocell fiber and other regenerated cellulose fibers. Holzforschung 63:18–22.

Yang, T.-C., Wu, T.-L., Hung, K.-C., Chen, Y.-L., Wu, J.-H. (2015) Mechanical properties and extended creep behavior of bamboo fiber reinforced recycled poly(lactic acid) composites using the time-temperature superposition principle. Constr. Build. Master. 93:558–563.

Yeo, S.S., Hsuan, Y.G. (2009) Predicting the creep behavior of high density polyethylene geogrid using stepped isothermal method. In: Service Life Prediction of Polymeric Materials: Global Perspectives. Eds. Martin, J.W., Ryntz, R.A., Chin, J., Dickie, R.A. Springer, New York. pp. 205–218.

Yeo, S.S., Hsuan, Y.G. (2010) Evaluation of creep behavior of high density polyethylene and polyethylene-terephthalate geogrids. Geotext. Geomembr. 28:409–421.

Yu, Y., Tian, G., Wang, H., Fei, B., Wang, G. (2011) Mechanical characterization of single bamboo fibers with nanoindentation and microtensile technique. Holzforschung 65:113–119.

Zhang, F., Endo, T., Qiu, W., Yang, L., Hirotsu, T. (2002) Preparation and mechanical properties of composite of fibrous cellulose and maleated polyethylene. J. Appl. Polym. Sci. 84: 1971–1980.